Particle Image Velocimetry to Evaluate Pulse Wave Velocity in Aorta Phantom with the lnD–U Method

Anaïs Moravia, Serge Simoëns, Mahmoud El Hajem, Benyebka Bousaïd, Marine Menut, Pascale Kulisa, Patrick Lermusiaux, Nellie Della-Schiava

Title: Particle image velocimetry to evaluate pulse wave velocity in aorta phantom with the lnD-U method

Authors: Anaïs Moravia[1], Serge Simoëns[1], Mahmoud El Hajem[1], Benyebka Bou-Saïd[2], Marine Menut[3], Pascale Kulisa[1], Patrick Lermusiaux[4], Nellie Della-Schiava[4]

[1]Université de Lyon, INSA de Lyon, Ecole Centrale de Lyon, Université Claude Bernard Lyon 1, CNRS, LMFA UMR 5509, Villeurbanne, France

[2]Université de Lyon, CNRS, INSA de Lyon, LaMCoS UMR5259, Villeurbanne, France

[3]CISTEN, 66 Bd. N. Bohr, CS 52132, 69603 Villeurbanne, France

[4] Vascular and Endovascular Department, Hospices Civils de Lyon, Lyon, France

Abstract (251 words)

Purpose - Pulse Wave Velocity (PWV) is an indicator of arterial stiffness used in the prediction of cardiovascular disease such as atherosclerosis. Non-invasive methods performed with ultrasound probes allow one to compute PWV and aortic stiffness through the measurement of the aortic diameter (D) and blood flow velocity (U) with the lnD-U method. This technique based on *in vivo* acquisitions lacks validation since the aortic elasticity modulus cannot be verified with mechanical strength tests. *Method* - In the present study, an alternative validation is carried out on an aorta phantom hosted in an aortic flow simulator which mimics pulsatile inflow conditions. This *in vitro* setup included a Particle Image Velocimetry device to visualize flow in a 2D longitudinal section of the phantom, compute velocity fields (U), and track wall displacements in the aorta phantom to measure the apparent diameter (AD) variations throughout cycles. *Results* - The lnD-U method was then applied to evaluate PWV (5.92 ± 0.32 m/s) and calculate the Young's's modulus of the aorta phantom (0.66 ± 0.08 MPa). This last value was compared to the elasticity modulus (0.53 ± 0.07 MPa) evaluated with tensile strength tests on samples cut from the silicone phantom. *Conclusion* - Considering the uncertainties from the two methods, the measured elasticities are consistent and close to a 50-60 years old male aortic behavior. A comparison with *in vivo* data shows that the choice of silicone for the phantom material is a relevant and promising option to mimic the human aorta on *in vitro* systems.

Keywords: Pulse Wave Velocity, aorta, phantom, circulatory mock loop, Particle Image Velocimetry

Contact: Anaïs Moravia – email: anais.moravia@ec-lyon.fr
Address: Ecole Centrale Lyon – LMFA – 36 avenue Guy de Collongue 69134 Ecully, FRANCE

(2958 words)

1. Introduction

In vivo, aortic stiffness is associated with some pathologies such as atherosclerosis which is known to reduce arterial wall elasticity [1, 2]. Different techniques have been developed to investigate arterial stiffness, identify risky regions and predict the outbreak of cardiovascular diseases [3-5]. One of the most common method to evaluate arterial stiffness is the measurement of the pulse wave velocity (PWV). PWV is the velocity at which the blood pressure pulse travels through a vessel. This quantity depends on blood and aortic wall properties and can thus, provide information on those properties such as aortic stiffness which could indicate the development of a plaque. The measurement of pulse wave velocity (PWV) can be achieved with non-invasive techniques such as the two points Transits-Time (TT) method [6,7], the one-point PU-loop (pressure-velocity loop) method [8], and the similar QA (flowrate-area loop) method [9] and lnD-U (logarithm of the diameter and velocity) derived methods [10-12]. These methods are based on the study of the relationship between the flow velocity or flowrate in the aorta and aortic walls movements which can be investigated through pressure, aortic section area; and diameter changes at one location (one-point methods). "Two points" methods consist in measuring the pressure pulse in two locations of the arterial tree. Knowing the distance between these two points and measuring the time required for the pulse to travel between them, PWV can be calculated. This method can be difficult to implement since invasive tools are often needed, the distance measurement is not trivial, and a perfect synchronization of the two devices that measure the pressure pulse is required [13]. 4D-MRI (Magnetic Resonance Imaging) can be used to image the whole aorta but involve much more complex and expensive equipment [14] with a strong impact of temporal resolution on computed PWV [15].

Conversely with "two points" assessments, the lnD-U technique provides local stiffness information as a "one-point" measurement. It can be performed with a routine US-Doppler (UltraSound) exam and only requires computing the aortic diameter change and blood velocity. However, the main limitation in the lnD-U method is the lack of in-vivo validation [11,12]. The method is mainly based on the Bramwell-Hill equation [16] which states that PWV is proportional to the aorta pressure variation and inversely proportional to aortic area variation throughout a cardiac cycle. From this PWV value, the arterial stiffness can be estimated through the Moens-Korteweg equation which shows a relationship between PWV, blood density, aortic wall thickness, Young's modulus, and radius [17]. In vivo, directly deducing the arterial stiffness from PWV measurement is questionable since the actual Young's modulus is

difficult to verified with traditional mechanical characterization tests on the subject to validate the theory. Alternative experimental validations are proposed by comparing PWV evaluation through other methods such as TT-method [18] shear wave elastography or fluid-structure interaction simulations which showed good agreements [19,20,21]. It would be desirable to be able to validate the computed material elasticity from this *in vivo* method with classical mechanical testing such as tensile tests on the same material. Since this comparison is not achievable from *in vivo* to *ex vivo* testing on a living patient, an equivalent method could be implemented with *in vitro* models and aorta phantoms. This comparison was achieved in Zimmermann et al., 2021[15] with aorta phantoms, a circulatory mock loop, 4D-flow MRI intra-luminal pressure measurements, transit-time like PWV estimation and tensile tests. This last study provided a volumetric information on the aorta behavior thanks to 4D-MRI and shows large discrepancies in the Young's modulus based tensile tests and PWV estimation. The pressure amplitude inflow conditions were very wide (105-40 mmHg) compared to in vivo conditions with a strong diameter variation along the aorta compared to in-vivo conditions. These conditions impacted the constant aortic diameter approximation used in the Moens-Korteweg equation to calculate the Young's modulus from PWV which was not adapted in this case. In the current study, we will confine ourselves to 2D in-plane evaluation which can be related to traditional US-Doppler PWV measurement methodology in the way that we use 2D imaging in one location of the aorta where velocity and diameter change are computed [12, 11]. The main purpose of this article is to provide a methodology to measure PWV and phantom stiffness on an in vitro simulator. Future experiments could be conducted by introducing the bench in an MRI [15] or using US-Doppler on the phantom to mature the present technique and compare the limitations of each methods.

An *in vitro* aortic flow simulator was developed in Moravia et al., 2022 [21] to reproduce physiological pulsatile flow rates and pressures in an aorta phantom made up of silicone with a patient-specific geometry and realistic elasticity. A Particle Image Velocimetry (PIV) setup was implemented on the mock loop to visualize the flow and track the aortic wall displacements. PIV was used to capture instantaneous velocity fields in a flow in a plane which crossed the flow domain in a chosen location. Prior to the experiment, the fluid was seeded with particles that acted as tracers. 2D-2C PIV (2 dimensions – 2 components PIV) consisted in illuminating a 2D section in the flow with a laser sheet to enlighten the particles and take snapshots of their position to track their displacements and deduce the flow velocity field at any point of the plane. The PIV setup is used to simultaneously measure flow velocity and aorta apparent diameter (AD) variations along a cardiac cycle. This AD refers to an "in-plane" diameter observed at the

intersection between the PIV laser sheet and the aorta phantom in the longitudinal direction. The lnD-U method can then be applied to compute PWV and estimate the aorta phantom stiffness based on this AD and other phantom characteristics. The great advantage of this *in vitro* system is that the aorta phantom Young's modulus can then be measured with mechanical tensile tests [22] and compared to the previous results.

In the current paper, we provide tools and a methodology to perform those two measurements and to investigate the stiffness evaluated from PWV with the lnD-U method and mechanically measured elasticity modulus with tensile tests in this *in vitro* context with an aorta phantom. The measured PWV and Young's modulus were also compared to *in vivo* data from the literature to determine if the silicone material is a relevant choice to mimic aorta with phantoms. The present experimental simulator tried to reach a relevant degree of biofidelity to mimic aortic flow in an in vitro context knowing that a perfect portrayal is impossible. We believe to have reached a significant mimicking of important aortic flow features among which the Young's modulus of the phantom is fundamental for such fluid/solid interaction system. Note that all along the paper the equations are given without units, all the indicated quantities are in SI units.

2. Methods

2.1 The lnD-U method

In routine exams, the lnD-U method can be used to evaluate the local stiffness of the aorta. Conversely with the Transit-Time method which requires to image pulse wave at two distant locations (and thus averages the PWV on this whole distance), the lnD-U method can be performed in a single section of the aorta as a local evaluation. This technique relies on the study of the AD variation of the aorta in relation to the blood velocity at the same location throughout the cardiac cycle [11,12]. This relation result from the Bramwell-Hill equation [16] and the water-hammer relationship between the PWV, pressure, and flow velocity [10].

$$PWV = \frac{1}{2}\frac{dU}{dln(D)} \quad (1)$$

where U is the velocity of blood flow in the investigated section, D is the diameter of the aorta in the same section and the derivative is the time variation of U for dU and ln(D) for dln(D). This relation (equation 1) is only valid in unidirectional wave periods along the cardiac cycle. If reflective waves appear, the relation can no longer be applied. Methods to identify reflection-free periods in the cardiac cycle exist [11]. They are based on wavefront analysis of

the blood pressure or velocity waveform in the aorta. The study of the rate of pressure (here converted to diameter change $\frac{dD}{dt}$) provides information on the contribution of forward and backward wavefronts. As expressed in [11], wave intensity (WI) can be calculated with velocity and diameter time derivation to investigate the contribution of each wavefront direction (equation 2). Forward wavefronts have a positive contribution on the WI while backward wavefronts have a negative contribution. Locating positive peak in WI is an indicator of a predominant forward wavefront [11].

$$WI = \frac{dD}{dt}\frac{dU}{dt} \quad (2)$$

Studies have shown that backward waves have negligible effects on diameter and velocity variations at the two positive peaks of WI [11, 23, 24]. In most cases, these peaks (which indicate reflection-less periods) correspond to early and late systole but the boundary conditions can affect them. The wavefront analysis has to be conducted on the experimental simulator with its own boundary conditions to identify those reflection-less. Locating one or the two phases allows determining where backward wave contributions are negligible to apply equation 1 to the measured flow velocity and phantom diameter change. Finally, the Moens-Korteweg equation [17] sets the relationship between the Young's modulus and the PWV (equation 3).

$$PWV = \sqrt{\frac{Eh}{\rho D}} \quad (3)$$

where E is the Young's modulus of the aorta, h is the thickness of the aorta, ρ is the density of the fluid and D is the aorta diameter. Note that E, h, ρ and D are mean values on the region of interest (ROI) in the aorta where the PWV was calculated. In the present experiment, this region covered a length of 63.57 mm in the aorta along which these mean values are averaged. Regarding equation 3, the most variable parameter is the aortic diameter which is supposed to be constant but can actually strongly vary along a real aorta. The ROI was chosen to obtain the flow velocity field with PIV.

Finally, applying the lnD-U method requires for synchronized measurements of the velocity and the diameter change which can be difficult to achieve where two devices are used to measure these quantities. In the present study PIV was used to calculate both on the same set of data (the same images) which solves the synchronization issue.

2.2 Experimental setup

The experimental setup consists of a circulatory mock loop which mimics aortic circulation (figure 1). This aortic flow simulator generates realistic pulsatile flow rate and pressures in the aorta phantom. A compliant silicone aorta phantom based on a patient-specific geometry and a blood mimicking fluid (BMF) with realistic shear-thinning properties [25] were designed for the experiment. The BMF is a mixture of water (55.6% by weight), glycerol (37% by weight), xanthan gum (200 ppm), and NaCl (7.4% by weight) and was designed to match the refractive index (RI) of the phantom (RI = 1.4) to minimize optical distortion for the PIV measurements. The fluid had a density of 1146 $kg.m^{-3}$. The aorta geometry was extracted from a patient's CT-Scan (Computed Tomography) provided by the Hospices Civils de Lyon and approved by the hospital's ethic committee. The aorta phantom was designed by Segula Technologies with a molding technique and silicone injection. The exact type of silicone could not be communicated. Inflow conditions are shown in figure 2. Cheng et al,. 2003 [26] was taken as the reference for human abdominal aorta flowrates at rest. The Reynolds number at the systolic peak and Womersley numbers were set to 1171 and 16.3 respectively thanks to the mock loop controlling system. Moravia et al., 2022 [21] provides the details on the design and properties of the phantom, the BMF, the circulatory mock loop, and the pulsatile inflow conditions. Additional details on the setup are provided in the supplementary material 1. The technique of Particle Image Velocimetry (PIV) is used to compute velocity fields in different sections of the aorta phantom. The PIV system, configuration, and particles choice are described in Moravia et al., 2022 [21] and summarized in table 1. In the current experiment, a region-of-interest (ROI) was defined as the cross-section between the laser sheet and the inner part of aorta phantom (were the fluid flows). This ROI is located in the aorta longitudinal direction and in the straightest region of the phantom to minimize out-of-plane flow for the application of the lnD-U method. The laser sheet was placed to meet the centreline of the aorta model at the location were the higher diameter was detected. This region was chosen as the one where both the flow and the wall movement could be imaged in a 2D-plane. In other regions the tortuosity of the model limited the use of this 2D imaging technique.

2.3 PIV measurements and post-processing

The mock loop imposed a pulsatile flow rate and pressure in the aorta phantom [21] while a series of PIV measurements were performed on the ROI (indicated on figure 1). The measurements consisted of pairs of images to track the particles displacements between the 2 images of each pair. The imposed cardiac cycle period was of T = 804

ms. The camera acquired a total of 1000 pairs of images at a framerate of 10Hz with a time-lapse $\Delta t = 4$ ms between the two images of each pair. This method allowed one to generate a batch of images that described different instants throughout the imposed cardiac cycle. Moreover, knowing the cycle period and imaging frequency (10 Hz), all the images can also be located on the imposed cardiac cycle. The designed system enabled to trigger the PIV imaging at chosen instants in the cardiac cycle which allows to locate each measurement in the imposed cardiac cycle. This was achieved thanks to a synchronized pulse waveform generation and PIV triggering in the in-house LabVIEW program that controlled the simulator. For the cross-correlation computation, a unique $\Delta t = 4$ms was chosen to maintain a consistent particle displacement (5 to 20 pixels) between two images of a pair all along a cardiac cycle. Indeed, the flow velocity strongly varied along a cardiac cycle which involved a wide range a particle displacement from systole to diastole. Even though Δt could be shorter (down to 1ms) during the systolic phase, the main limitation came from the slow-motion diastolic phase with risks of capturing a zero displacement if Δt was too short. Thanks to preliminary experiments, $\Delta t = 4$ ms was found to suit all the cycle phases. The PIV setup and imaging parameters are summed up in Table 1. A total of 125 successive cycle were needed to acquire those 1000 pairs of images. To achieve those 1000 measurements, the work was divided into 5 series of dataset with 200 pairs of images each because of camera RAM limitations with such a high framerate. The inflow conditions and parameters were kept the same for each dataset to ensure reproducibility.

For each of the PIV images, the aorta apparent diameter and velocity fields were computed (figure 3). The outer diameter (D) of the aorta was estimated thanks to a MATLAB in-house program [21] thanks to aorta phantom upper and lower wall detection with digital image treatments and analyses (based on grey scale transitions on the images). Additional details on the algorithm are provided in the supplementary material 2. The velocity fields were calculated with the software Davis 10 (LaVision). With Davis 10, the image cross-correlation was conducted with a multipass method in the ROI to calculate the velocity field (figure 3). The first pass was performed with 32x32 pixels interrogation windows with an ellipsoid weight with the long axis in the main flow direction x and a 0% overlap. the second pass was reduced to 16x16 pixels interrogation windows with a round Gaussian weight and an overlap of 50%. For each velocity field, a 2^{nd} order polynomial interpolation algorithm was applied to fill up missing vectors (less than 1% of vectors) and was followed by a 3x3 smoothing filtering. The 16x16 pixels interrogation windows have an equivalent resolution of 0.40x0.40 mm^2 knowing that the mean aorta diameter is about 32.1 mm. This mean value on the ROI and throughout the cardiac cycle was calculated as an “in-plane” diameter with the PIV images (intersection

between the laser sheet and the phantom). The signal to noise ratio is limited by the value chosen as classically for PIV analysis.

2.4 Tensile strength tests

The silicone phantom elasticity is measured through uniaxial tensile strength tests performed on 8 samples cut from a sacrificial aorta phantom. This sacrificial phantom is the same model as the one used in the mock loop (same geometry, silicone and manufacturing technique). The pre-condition for each sample was set to 10N and the loading was achieved with 1mm/s jaw displacements to keep conditions. From those samples, the phantom wall thickness was measured as h = 2.19 ± 0.42 mm (mean and standard deviation over the 8 samples). The tests were performed on a Lloyd LF-Plus machine and combined with a Digital Image Correlation measurement [22,27]. A random speckle pattern was applied on the sample and a camera captured their displacement with the tensile machine gripped jaws movement. The cross-correlation on the speckle displacement was computed with the software VIC-3D (Correlated Solution). Knowing the displacement and the force applied for the jaw displacements, the elastic modulus could be calculated with the longitudinal Lagrangian strain [22,28, 29].

3. Results

The mean D, along the aorta and the mean velocity (U) on the whole ROI were calculated for each pair of images (equation 4 and 5). The mean velocity was integrated on the volume based on the 2D measured velocity in the ROI and with a cylindrical symmetry approximation.

$$D = \frac{1}{n_y}\sum_i^{ROI} D_i \qquad (4)$$

$$U = \left(\sum_{i,j}^{ROI} u_{i,j} \,.\, r_j\right) . \frac{ds}{L \,.\, \left(\frac{D}{2}\right)^2} \qquad (5)$$

where D_i was the AD computed at each of the n_y vertical line of the ROI with index i along the x-axis, n_y is the total number of vertical lines, $u_{i,j}$ was the velocity on each interrogation windows inside the ROI (figure 3) at a corresponding radius r_j in the phantom, ds is the surface of a pixel and L is the length of the ROI. D and U waveform are shown in figure 4.a on a cardiac cycle timeline. To rescale the D and U data on a cardiac cycle timeline (T = 804 ms), the datasets were rescaled knowing the 10Hz imaging frequency and location of the first image on the imposed cardiac cycle. The corresponding wave intensity (WI) was then computed and plotted in figure 4.b to detect local maxima. The early systole maximum was identified as the first peak [23] and indicated in red on the graph. This

period was thus considered to be a reflection-free one where the diameter / velocity relationship could be analyzed to calculate PWV.

The lnD-U loop graph is provided in figure 5.a for the full set of 1000 pairs of images. The cycle showed a similar shape as in Di Lascio et al., 2014 [11] where the experiment was conducted on mice with ultrasound measurements. To compute PWV, the data corresponding to the early systole (reflection-free period identified with the WI analysis) were isolated and presented in figure 5.b. The linear regression was performed on those selected data and the slope gives the $\frac{dlnD}{dU}$ factor. From equation 1, the calculated PWV was 5.79 ± 0.33 m/s. The uncertainty was evaluated from linear regression standard error on the slope parameter.

Thanks to the Moens-Korteweg equation (equation 3), the Young's modulus was computed knowing that the aorta wall thickness was h = 2.19 ± 0.42 mm, the blood mimicking fluid's density was ρ = 1146 kg.m^{-3} and the aorta mean AD = 32.1 mm. This diameter was set as the mean diameter in the ROI (equation 4) which was then averaged on the whole cardiac cycle. As a result, the computed Young's modulus was E_{lnD-U} = 0.56 ± 0.12 MPa. The uncertainty was evaluated with the uncertainty propagation formulation on equation 3 that took into account the error from the PWV calculation (standard error of the linear regression coefficient) and the wall thickness h (refer to supplementary material 3).

The Young's modulus calculated from the tensile strength tests was equal to $E_{tensile}$ = 0.53 ± 0.07 MPa (the error is the standard deviation between the 8 measured samples). Considering the uncertainties of each method, the two values (E_{lnD-U} and $E_{tensile}$) were consistent with each other. Uncertainties for the present method, E_{lnD-U} , came from PIV measurements and from the silicone manufactured walls. These last ones are common to the ones used for $E_{tensile}$. The tensile technique has its own uncertainties. It is thus interesting to note that the use of tensile technic or PIV technic provides similar uncertainties which is cumulative with the ones coming from silicone manufacturing. The ideal solution would be to first conduct PIV measurements at one location and second, to cut some sample from the wall at the exact same location to perform the tensile tests. However, the price of silicone phantom was sufficiently high not to sacrifice all our phantoms in tensile tests. Another point is that the tensile method supposed anisotropy. Such hypothesis has to be tested in the future and some departure could be responsible of some differences.

4. Discussion

In the current study, PWV and aorta phantom Young's modulus were measured with the local lnD-U loop method applied on flow velocity and diameter variations data obtained with PIV. For PWV and both Young's modulus computations, the results were compared to typical data from human aortas. Concerning PWV, the value of 5.79 ± 0.33 m/s was in the range of an abdominal aorta for a normal subject of about 50 years old [20, 30]. The young's modulus was also in the range of measured elasticities of human aortas according to Lang et al., 1994 [31] with typical values ranging from 0.25 to 1.7 MPa. Moreover, under the realistic pulsatile conditions imposed by the mock loop, the phantom diameter variation was around ΔD = 0.8 mm which was in accordance of a 53-69 years old male ΔD [32]. In the field of *in vitro* simulator where rigid glass [33], 3D-printed [15] and silicone [34] models are used, the aorta phantom made up of silicone appeared as a relevant choice to mimic those aorta phantom mechanical responses to pulsatile flow.

Regarding the E_{lnD-U} and $E_{tensile}$ comparison, the values were in accordance regarding the uncertainty factors. The percentage difference between the two values was 5.6%. As noted above uncertainties were various and some were inherent to the different techniques. To provide an order of magnitude, when calcification occurs in the aorta and atherosclerosis develops, the Young's modulus of the arterial wall can double and even become ten times higher in sever calcification cases compared to a healthy aorta [34]. In the current study, the difference in the measured E values were provided large uncertainties but remains in the range of realistic human aorta stiffness. Moreover, the measurements were based on 'in-plane" values giving flow velocity components. The out-of-plane flow is source of a bias error, linked to the plane thickness and responsible for an increase of particle pattern differences from one frame to the other. That is limited via the time step recording between two frames and acceptable signal to noise ratio fixed during cross correlation analysis. To go further, the technique of 3D-PTV (particle tracking velocimetry) can be used to calculate the velocity with three velocity component determination in our region-of-interest but in a volume [36]. This method involves multiple cameras and the use of a laser volume instead of a laser sheet to illuminate the targeted region which could be adapted to the existing experimental bench but with a rather more complex data analysis. Global diameter and velocity change on the whole volume could provide a more precise PWV evaluation [15]. Finally, changing the boundary conditions to modify wave reflections and inflow conditions could help testing the limits of this lnD-U technique to evaluate elastic properties and test the robustness of this method with the help of the WI calculation to identify reflection-less phases. In any case, the same PIV measurements can be applied to

simultaneously compute the flow velocity and diameter change on multiple planes and/or other phantoms with the current aortic flow simulator and the imaging methodology.

The main limitation with lnD-U method applied with our PIV system comes from the AD detection. As explained previously, each point presented on the lnD-U loop corresponded to a single pair of images. The statistics relied on large series of single pair of images shot randomly throughout the cardiac cycle. As a consequence, in the present experiments, we count on a large amount of random data on the period of interest (early systole) to guaranty a reliable linear regression to compute the $\frac{dlnD}{dU}$ slope parameter. On a pair of images, the most difficult value to compute is the AD, since punctual wall detection defects can occur due to the presence of foreign body and light reflection in the field of view (mostly in the background). The in-house algorithm is based on grey scale value differences between the dark background and the lighter phantom. Strong disturbance on the background or micro-bubble deposit on the phantom surface can cause incorrect localization of the phantom's walls (refer to supplementary material 2). A way to improve the technique would be to optimize the wall detection algorithm.

In the current set of data, 1000 pairs of images were shot but only 109 of them were in the early systole (reflexion-less) period (10.9%). However, a complete cycle imaging was necessary to conduct the WI analysis and identify this reflexion-less period. The PIV setup parameters or the implementation of a fast PIV device could help focusing the imaging in this particular period.

Finally, the current patient-specific aorta phantom was designed to reach a constant wall thickness while the human aorta has a non-uniform wall thickness [37]. Specific protocol should be developed to extract the corresponding patient's aorta thickness and to implement it on the manufacturing technique. It could provide more relevant models and influence the results. The current observations, calculations and conclusions are all based on the uniform wall-thickness hypothesis which differs from real patients and our aorta phantom. The Moens-Korteweg is based on this hypothesis which can limit the accuracy of the resulting Young's modulus.

5. Conclusion

An *in vitro* investigation of the lnD-U method was achieved on a circulatory mock loop which replicates pulsatile flow rates and pressure conditions in an abdominal aorta phantom made up of silicone. The lnD-U method often lacks validation with traditional tensile test to measure material elasticity. The current experiment on the aorta phantom is used to compare the lnD-U method to compute Young's modulus and traditional tensile test evaluation. Consistent Young's modulus values were found between the lnD-U and the tensile tests methods with a 5.6% difference but not

sufficient to validate the theory on the relation between PWV and arterial stiffness. Errors can emerge from out-of-plane flow, wall thickness approximation and diameter change evaluation. Further investigation conducted on other phantom sections or other phantom geometries with the same silicone material are necessary to validate this lnD-U method with larger statistics than this single case. However, the current benchtop simulator and imaging methodology can be implemented for further investigation of the lnD-U technique and test the robustness of this method by varying boundary conditions (connectors, inflow conditions, peripheral resistance with valves, etc.). The same methodology can be implemented on those future cases and the system could also be used for other method comparisons such as the TT or PU-loop method.

Acknowledgements

This project is granted by AURA region under the label Pack ambition 2018 @NEDA (18001168001). The tensile tests were performed by Marine Menut et Laurie Portero in LaMCoS (INSA de Lyon).

Conflict of interest

Anaïs Moravia, Serge Simoëns, Mahmoud El Hajem, Benyebka Bou-Saïd, Marine Menut, Pascale Kulisa, Patrick Lermusiaux and Nellie Della-Schiava declare that they have no conflicts of interest.

References

[1] Van Popele, N. M., Grobbee, D. E., Bots, M. L., Asmar, R., Topouchian, J., Reneman, R. S., ... & Witteman, J. C. (2001). Association between arterial stiffness and atherosclerosis: the Rotterdam Study. Stroke, 32(2), 454-460. https://doi.org/10.1161/01.STR.32.2.454

[2] Mackey, R. H., Venkitachalam, L., & Sutton-Tyrrell, K. (2007). Calcifications, arterial stiffness and atherosclerosis. Atherosclerosis, Large Arteries and Cardiovascular Risk, 44, 234-244. https://doi.org/10.1159/000096744

[3] Mackenzie, I. S., Wilkinson, I. B., & Cockcroft, J. R. (2002). Assessment of arterial stiffness in clinical practice. Qjm, 95(2), 67-74. https://doi.org/10.1093/qjmed/95.2.67

[4] Oliver, J. J., & Webb, D. J. (2003). Noninvasive assessment of arterial stiffness and risk of atherosclerotic events. Arteriosclerosis, thrombosis, and vascular biology, 23(4), 554-566. https://doi.org/10.1161/01.ATV.0000060460.52916.D6

[5] Segers, P., Rietzschel, E. R., & Chirinos, J. A. (2020). How to measure arterial stiffness in humans. Arteriosclerosis, thrombosis, and vascular biology, 40(5), 1034-1043. https://doi.org/10.1161/ATVBAHA.119.313132

[6] Vulliémoz, S., Stergiopulos, N., & Meuli, R. (2002). Estimation of local aortic elastic properties with MRI. Magnetic Resonance in Medicine: An Official Journal of the International Society for Magnetic Resonance in Medicine, 47(4), 649-654. https://doi.org/10.1002/mrm.10100

[7] Bargiotas, I., Mousseaux, E., Yu, W. C., Venkatesh, B. A., Bollache, E., De Cesare, A., ... & Kachenoura, N. (2015). Estimation of aortic pulse wave transit time in cardiovascular magnetic resonance using complex wavelet cross-spectrum analysis. Journal of Cardiovascular Magnetic Resonance, 17(1), 1-11. https://doi.org/10.1186/s12968-015-0164-7

[8] Khir, A. W., O'brien, A., Gibbs, J. S. R., & Parker, K. H. (2001). Determination of wave speed and wave separation in the arteries. Journal of biomechanics, 34(9), 1145-1155. https://doi.org/10.1016/S0021-9290(01)00076-8

[9] Rabben, S. I., Stergiopulos, N., Hellevik, L. R., Smiseth, O. A., Slørdahl, S., Urheim, S., & Angelsen, B. (2004). An ultrasound-based method for determining pulse wave velocity in superficial arteries. Journal of biomechanics, 37(10), 1615-1622. https://doi.org/10.1016/j.jbiomech.2003.12.031

[10] Feng, J., & Khir, A. W. (2010). Determination of wave speed and wave separation in the arteries using diameter and velocity. Journal of biomechanics, 43(3), 455-462. https://doi.org/10.1016/j.jbiomech.2009.09.046

[11] Di Lascio, N., Stea, F., Kusmic, C., Sicari, R., & Faita, F. (2014). Non-invasive assessment of pulse wave velocity in mice by means of ultrasound images. Atherosclerosis, 237(1), 31-37. https://doi.org/10.1016/j.atherosclerosis.2014.08.033

[12] Negoita, M., Hughes, A. D., Parker, K. H., & Khir, A. W. (2018). A method for determining local pulse wave velocity in human ascending aorta from sequential ultrasound measurements of diameter and velocity. Physiological measurement, 39(11), 114009.

[13] Weber, T., Ammer, M., Rammer, M., Adji, A., O'Rourke, M. F., Wassertheurer, S., ... & Eber, B. (2009). Noninvasive determination of carotid–femoral pulse wave velocity depends critically on assessment of travel distance:

a comparison with invasive measurement. Journal of hypertension, 27(8), 1624-1630.

[14] van Elderen, S. G., Westenberg, J. J., Brandts, A., van der Meer, R. W., Romijn, J. A., Smit, J. W., & de Roos, A. (2011). Increased aortic stiffness measured by MRI in patients with type 1 diabetes mellitus and relationship to renal function. AJR-American Journal of Roentgenology, 196(3), 697.

[15] Zimmermann, J., Loecher, M., Kolawole, F. O., Bäumler, K., Gifford, K., Dual, S. A., ... & Ennis, D. B. (2021). On the impact of vessel wall stiffness on quantitative flow dynamics in a synthetic model of the thoracic aorta. Scientific Reports, 11(1), 1-14. https://doi.org/10.1038/s41598-021-86174-6

[16] Bramwell, J. C., & Hill, A. V. (1922). The velocity of pulse wave in man. Proceedings of the Royal Society of London. Series B, Containing Papers of a Biological Character, 93(652), 298-306. https://doi.org/10.1098/rspb.1922.0022

[17] Tijsseling, A. S., & Anderson, A. (2012). CASA-Report 12-42 December 2012. ISSN: 0926-4507

[18] Khir, A. W., Swalen, M. J. P., Feng, J., & Parker, K. H. (2007). Simultaneous determination of wave speed and arrival time of reflected waves using the pressure–velocity loop. Medical & biological engineering & computing, 45(12), 1201-1210.

[19] Shahmirzadi, D., Li, R. X., & Konofagou, E. E. (2012). Pulse-wave propagation in straight-geometry vessels for stiffness estimation: theory, simulations, phantoms and in vitro findings. Journal of biomechanical

[20] Grotenhuis, H. B., Westenberg, J. J., Steendijk, P., van der Geest, R. J., Ottenkamp, J., Bax, J. J., ... & de Roos, A. (2009). Validation and reproducibility of aortic pulse wave velocity as assessed with velocity-encoded MRI. Journal of Magnetic Resonance Imaging: An Official Journal of the International Society for Magnetic Resonance in Medicine, 30(3), 521-526. https://doi.org/10.1002/jmri.21886

[21] Moravia, A., Simoëns, S., El Hajem, M., Bou-Saïd, B., Kulisa, P., Della-Schiava, N., & Lermusiaux, P. (2022). In vitro flow study in a compliant abdominal aorta phantom with a non-Newtonian blood-mimicking fluid. Journal of biomechanics, 130, 110899. https://doi.org/10.1016/j.jbiomech.2021.110899

[22] Palanca, M., Tozzi, G., & Cristofolini, L. (2016). The use of digital image correlation in the biomechanical area: a review. International biomechanics, 3(1), 1-21. https://doi.org/10.1080/23335432.2015.1117395

[23] Jones, C. J., Sugawara, M., Kondoh, Y., Uchida, K., & Parker, K. H. (2002). Compression and expansion wavefront travel in canine ascending aortic flow: wave intensity analysis. Heart and vessels, 16(3), 91-98. https://doi.org/10.1007/s003800200002

[24] Harada, A., Okada, T., Niki, K., Chang, D., & Sugawara, M. (2002). On-line noninvasive one-point measurements of pulse wave velocity. Heart and vessels, 17(2), 61-68. https://doi.org/10.1007/s003800200045

[25] Thurston, G. B. (1979). Rheological parameters for the viscosity viscoelasticity and thixotropy of blood. Biorheology, 16(3), 149-162.

[26] Cheng, C. P., Herfkens, R. J., & Taylor, C. A. (2003). Comparison of abdominal aortic hemodynamics between men and women at rest and during lower limb exercise. Journal of vascular surgery, 37(1), 118-123.

[27] Litlzer, S., & Vezin, P. (2012, September). Characterization of the intima layer of the aorta by Digital Image Correlation in dynamic traction up to failure. In Proceedings of the International Research Council on the Biomechanics of Injury conference (Vol. 40, pp. 650-661). International Research Council on Biomechanics of Injury.

[28] Raghavan, M. L., Webster, M. W., & Vorp, D. A. (1996). Ex vivo biomechanical behavior of abdominal aortic aneurysm: assessment using a new mathematical model. Annals of biomedical engineering, 24(5), 573-582. https://doi.org/10.1007/BF02684226

[29] Menut M, Bou-Said B, Walter-Le Berre H, Vezin P, Ben Boubaker L (2015) Characterization of the Mechanical Properties of the Human Aortic Arch Using an Expansion Method. J Vasc Med Surg 3: 188.

[30] Devos, D. G., Rietzschel, E., Heyse, C., Vandemaele, P., Van Bortel, L., Babin, D., ... & Achten, R. (2015). MR pulse wave velocity increases with age faster in the thoracic aorta than in the abdominal aorta. Journal of Magnetic Resonance Imaging, 41(3), 765-772. https://doi.org/10.1002/jmri.24592

[31] Lang, R. M., Cholley, B. P., Korcarz, C., Marcus, R. H., & Shroff, S. G. (1994). Measurement of regional elastic properties of the human aorta. A new application of transesophageal echocardiography with automated border detection and calibrated subclavian pulse tracings. Circulation, 90(4), 1875-1882.

[32] Sonesson, B., Länne, T., Vernersson, E., & Hansen, F. (1994). Sex difference in the mechanical properties of the abdominal aorta in human beings. Journal of vascular surgery, 20(6), 959-969. https://doi.org/10.1016/0741-5214(94)90234-8

[33] Deplano, V., Knapp, Y., Bertrand, E., & Gaillard, E. (2007). Flow behaviour in an asymmetric compliant experimental model for abdominal aortic aneurysm. Journal of biomechanics, 40(11), 2406-2413.

[34] Deplano, V., Knapp, Y., Bailly, L., & Bertrand, E. (2014). Flow of a blood analogue fluid in a compliant abdominal aortic aneurysm model: Experimental modelling. Journal of biomechanics, 47(6), 1262-1269.

[35] Mouktadiri, G., & Bou-Saïd, B. (2013). Aortic endovascular repair modeling using the finite element method. Journal of biomedical science and engineering, 2013.

[36] Gülan, U., Lüthi, B., Holzner, M., Liberzon, A., Tsinober, A., & Kinzelbach, W. (2012). Experimental study of aortic flow in the ascending aorta via particle tracking velocimetry. Experiments in fluids, 53(5), 1469-1485.

[37] Concannon, J., Dockery, P., Black, A., Sultan, S., Hynes, N., McHugh, P. E., ... & McGarry, J. P. (2020). Quantification of the regional bioarchitecture in the human aorta. Journal of anatomy, 236(1), 142-155. https://doi.org/10.1111/joa.13076engineering, 134(11).

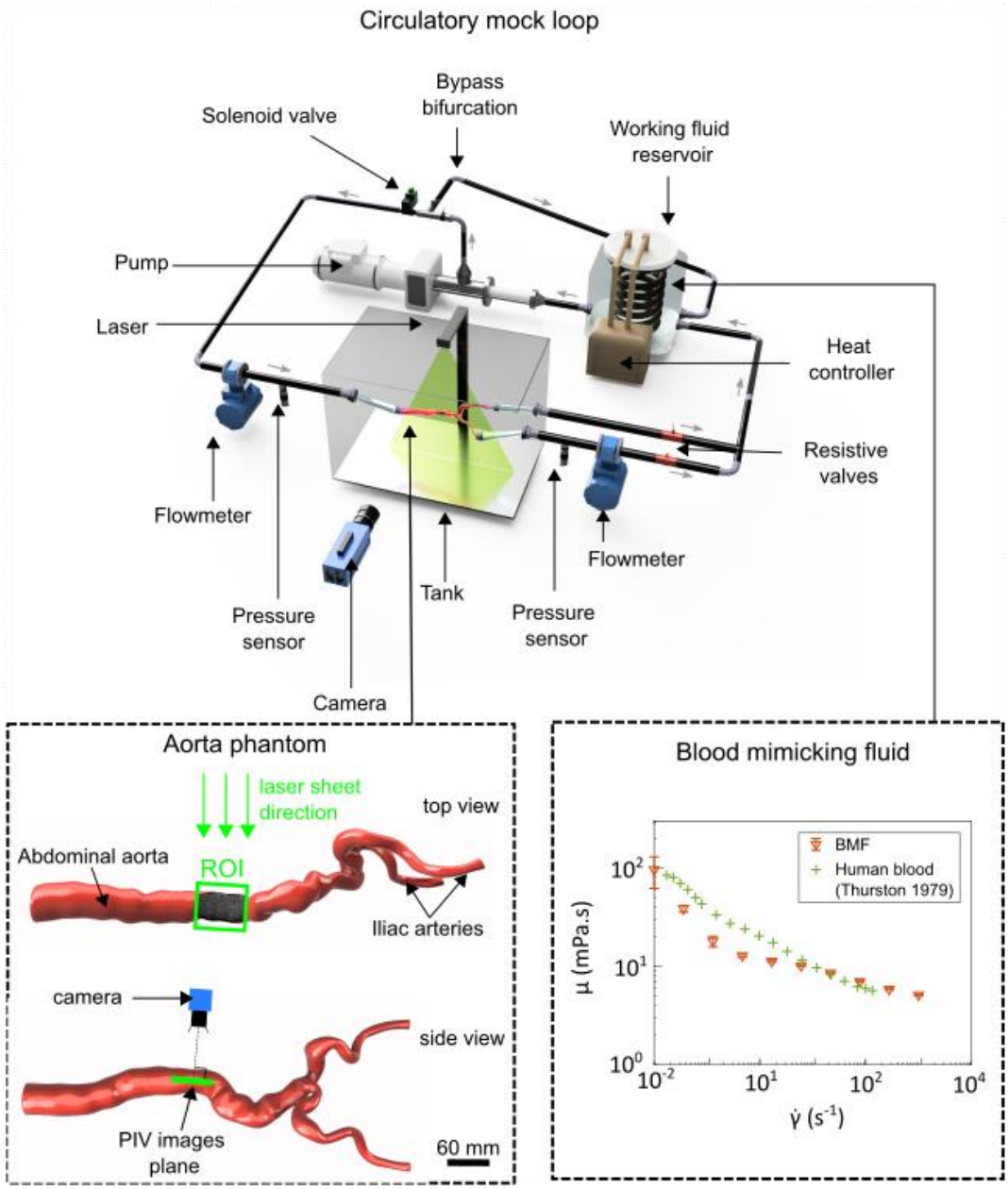

Fig.1 Experimental setup with the circulatory mock loop hosting the aorta phantom and conveying the blood mimicking fluid (BMF). The Regions of interest (ROI) corresponds to the imaged PIV plane with the camera and is located in the longitudinal direction of the phantom at the maximum of diameter. The BMF viscosity measurements are provided for different shear rates [18] (with human blood reference [22])

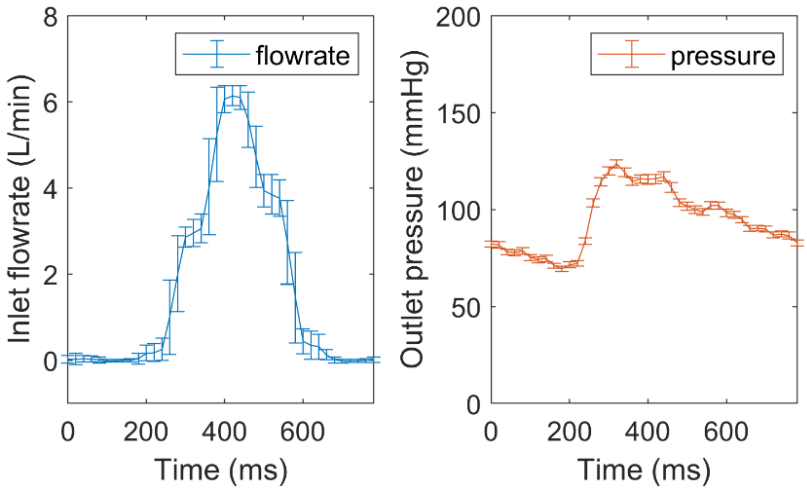

Figure 2: Inlet flowrate and outlet pressure on the experimental setup. The flowrate amplitude was set to meet the data from Cheng et al. 2003 (abdominal aorta flowrate measurements). Note that the inlet flowrate is measured in a rigid pipe upward from the compliant phantom and can only detect flow in the main direction (toward the phantom). A dampening effect on the curve and backflows are observed in the phantom but cannot be captured by this flowmeter. The standard deviation is indicated for the 125 successive cycles needed for the experiment.

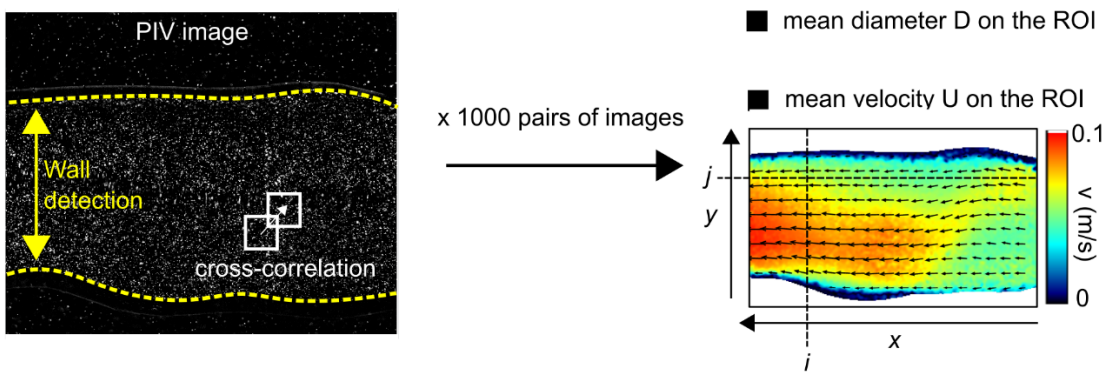

Fig.3 Illustration of the lnD-U method applied on the PIV images thanks to mean diameter and mean velocity computation on the ROI. Refer to the bottom left box on figure 1 for the orientation of the camera an image compared to the aorta position and flow main direction (from the abdominal aorta toward the iliac arteries)

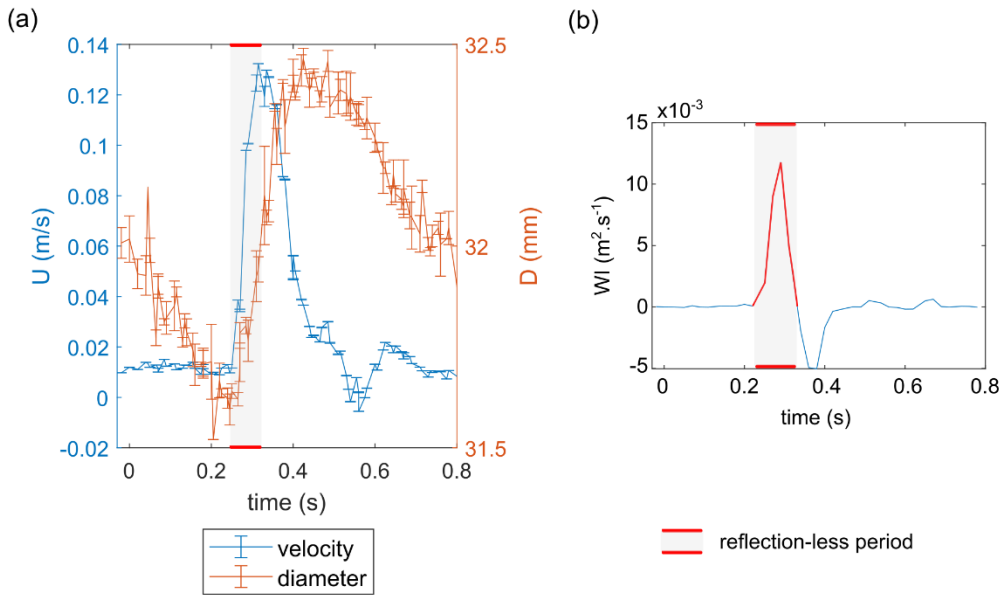

Fig.4 (a) Mean diameter and velocity waveform in the ROI throughout time rescaled on a cardiac cycle period, (b) WI was calculated and a local maximum was identified (red part from t = 0.22 to 0.33 ms is the cardiac cycle timelapse). The two other visible maxima will not be considered in this analysis.

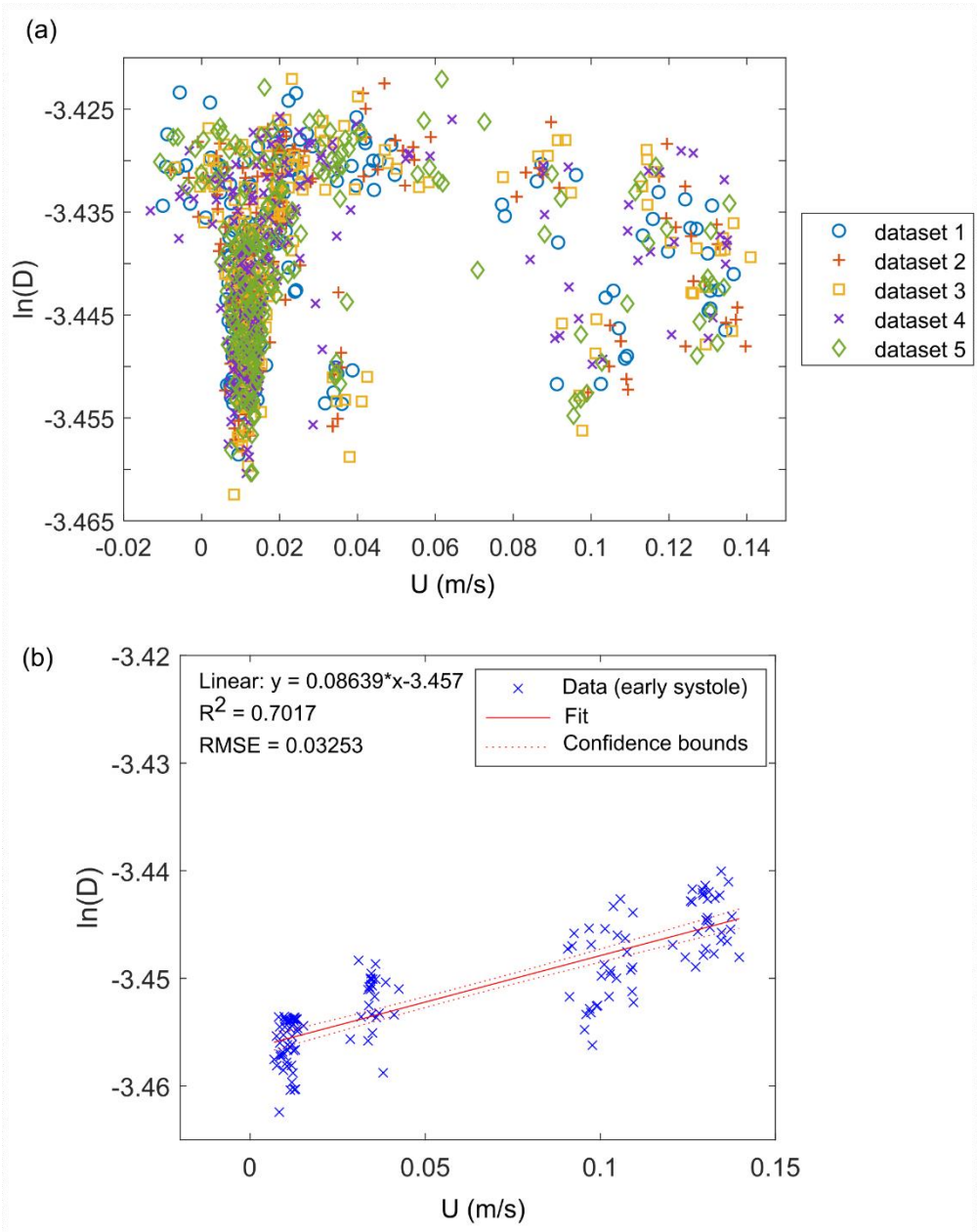

Fig.5 (a) lnD-U loop graph for 5 datasets of 200 images each (total of 1000 pairs of images). Each dataset corresponds to PIV measurements in the ROI, shot with the same imaging parameters. (b) Curve fit on data corresponding to the increase in systole (109 images) where WI showed a local maximum

Setup element	**Reference**
Laser type	Nd:YAGnanoPIV, λ = 532 nm, Litron laser
Camera	sCMOS, 2560 x 2160 pixels, LaVision
Lens	AF Micro-Nikkor 60mm f/2.8D, Nikon
Particles	PMMA-RhB, d = 1 190 $kg.m^{-3}$, LaVision
	Parameters
Laser sheet thickness (mm)	1
PIV framerate (Hz)	10
Δt between pulses (ms)	4
Field-of-view (mm x mm)	63.57 x 53.37
Interrogation window (pixel x pixel)	16 x 16
Interrogation window (mm x mm)	0.40 x 0.40

Table 1: PIV set up and parameters

Supplementary material 1: Experimental setup

The main element of the experimental simulator was the aorta phantom with is a scale model of a patient's aorta geometry. The phantom was immersed in a tank containing a fluid with the same refractive index than the working fluid (BMF). The fact that the tank was filled up with a fluid had two purposes: (1) to minimize optical distortions with an homogenised refractive index media (BMF, phantom and tank fluid) and (2) to apply a certain pressure on the aorta phantom to mimic its surrounding environment. When immersed in the tank, the aorta phantom was lying on a support that mimics the shape of a backbone and to stabilize the model when subjected to pulses.

In the tank the aorta is connected to the main loop thanks to rigid hose connector. Note that any change in the boundary conditions, rigidity of the connector or configuration of the mock loop pipe with influence the way the pulse waveform reflects in the loop. The lnD-U method is based on the hypothesis of unidirectional wavefront analysis as specified in the article. Therefore, a new WI analysis should be conducted if the mock loop and inflow conditions are modified to locate the reflection-less phases.

The PIV setup configuration allowed to generate a 2D laser sheet emitted from the top of the tank which enlighten a section visible from the side of the tank as indicated in figure 1 from the main text. When imaging flows in "tubes" with such tortuosity the main problem with 2D-PIV is to find positions where a 2D plane can pass and where most of the mass flux is captured.

In the hypothesis of equation (5), converting 2D n-plane to 3D flow could become a source of large bias when the transverse velocity (out-of-plane) is not negligible compared to the longitudinal one (in plane). 3D-PTV studies would allow to quantify this bias. In the current study, this bias was indirectly checked by comparing the mass flux computed with PIV and the one provided by the inlet flowmeter which integrated flow on the whole section. We observed a 13% underestimation of mass flux with the PIV compared to the inlet flowmeter. The conclusion was that the in-plane flow is not sufficient to estimate the whole flow in the aorta phantom and is only an approximation.

Supplementary material 2: Wall detection algorithm

The wall detection algorithm allowed to detect the position of the outer wall of the aorta phantom based on greyscale difference between the dark background and the lighter wall. The results of this algorithm were first used in Moravia et al., 2022 to track wall displacement in the same aorta phantom but in another region of the model.

The phantom walls were compliant and moved with a periodic pattern when pulsatile flowrate and pressure was imposed in the circuit. The detection was conducted with a in-house MATLAB program using a threshold to differentiate the background from the wall. A Morphological closing filter is than applied on the image to deal with foreign elements that can be present in the background. Indeed, the phantom is immersed in a tank and some bubbles, fibres of PIV particle can fly in the background. These elements visible in figure S2 result from small leakages or the presence of air in the mock loop when installing the phantom prior to the experiment.

In our case the threshold was sat to 555 greyscale level for our 64 bits images and the closing algorithm was operated rectangular patch of 5x5 pixels. These values can vary depending on the lightening and the resolution of the images.

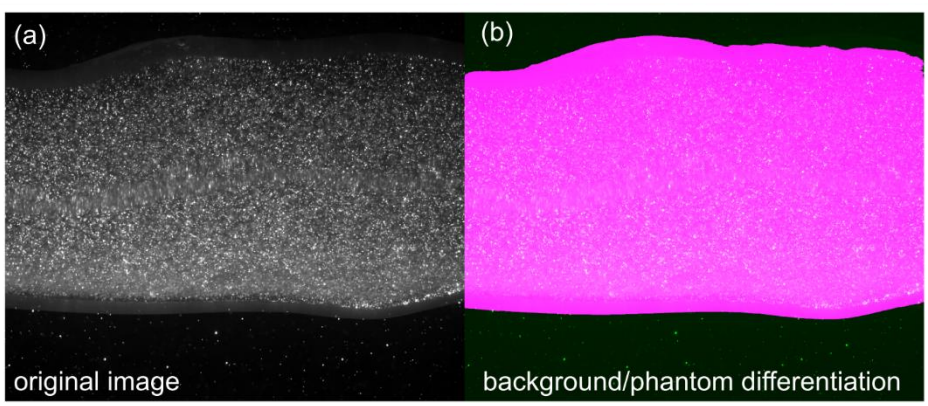

Figure S2-1: Example of an outer wall detection with the threshold algorithm. (a) shows the original PIV image and (b) shows the separated phantom region from the background. This computation in conducted on the whole set of images to follow the wall displacement throughout the cardiac cycle.

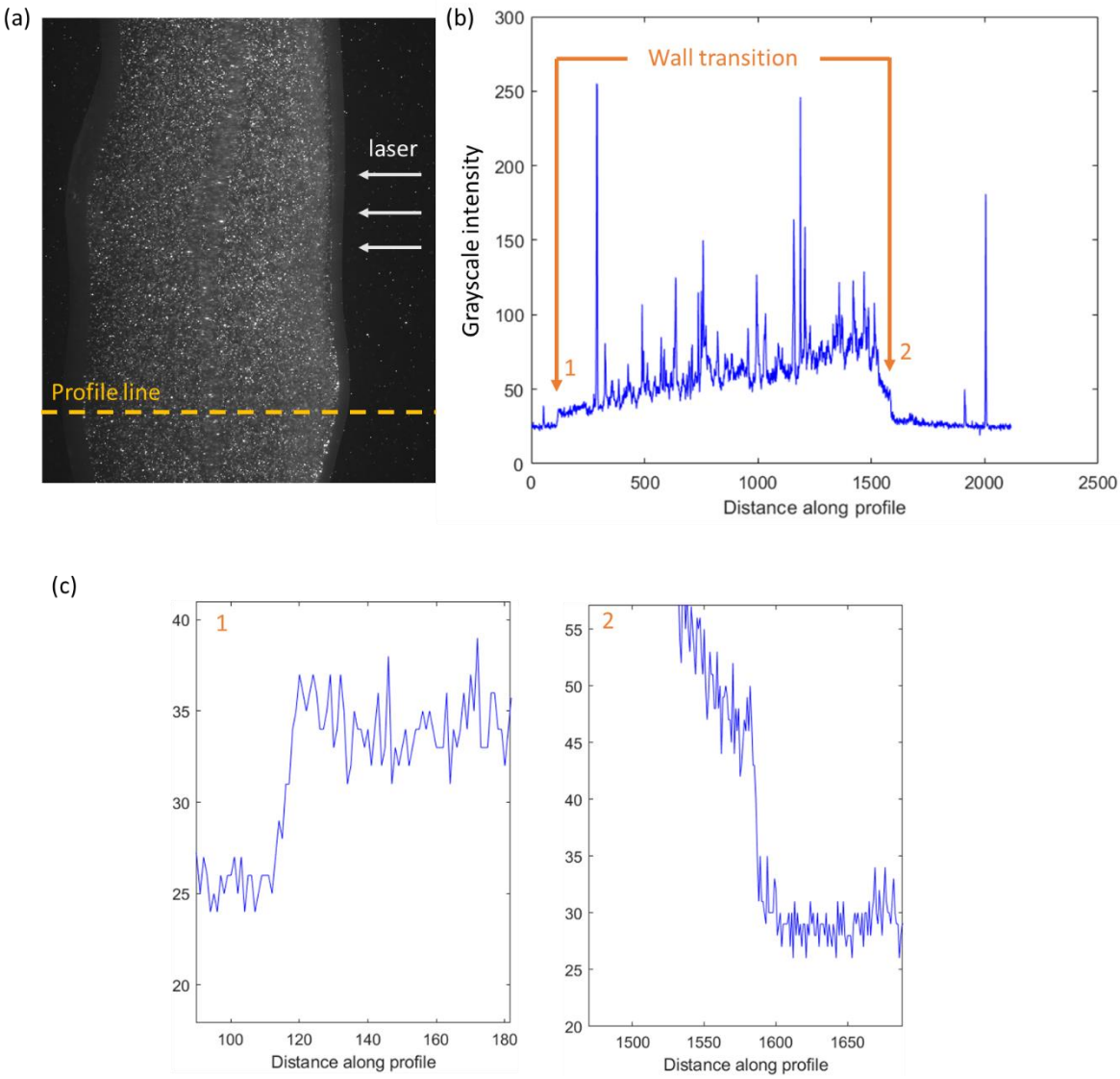

Figure S2-2: Example an intensity profile line on a PIV image. The wall transition indicated when the background ends and the wall begin. To separate the phantom from the background, a threshold algorithm was used isolate grayscale over this transition.

Figure S2-2 shows an intensity profile on the aorta phantom. Depending on the location on the phantom, the intensity transition is typically observed in 2 to 3 pixels along the profile which corresponds to 0.050 to 0.075 mm (). On the opposite side of the laser (lower light), the transition takes 3 to 5 pixels along the profile (0.075 to 0.12 mm) knowing that the diameter variation is about 0.8 mm.

A mentioned in the discussion, some particles or air bubbles punctually deposit on the outer wall. PIV particles size are between 0.020 and 0.50 mm which will affect the near wall light intensity transition and add extra error on the diameter estimation.

.

Not that the program also allowed to detect small vibrations of the system. When running the mock loop small vibrations are observed in the circuit and in the aorta phantom because of the pump running. Thanks to multiple imaging in different regions of the phantom the vibration were quantified as displacements up to 3 pixels in the phantom. This quantity is provided for the current article field-of-view size. The program can differentiate contraction (upper and lower get closer), dilatation (upper and lower border diverge) and vibration (shift of the upper and lower wall in the same direction in a range of 3 pixels) of the phantom.

Supplementary material 3: Uncertainty calculation

The Moens-Korteweg equation gives a relationship between the PWV and the Young's modulus E such that:

$$E = \frac{PWV^2\ \rho\ D}{h}$$

This equation is a power and product type where letters Q, x, y and z represent physical quantities and ΔQ $\Delta x, \Delta y$ and Δz their uncertainties:

$Q = x^m y^n \dots z^p$

The propagation uncertainty formulation takes into account product and power factors thanks to the following formula:

$$\frac{\Delta Q}{|Q|} = \sqrt{\left(|m|\frac{\Delta x}{|x|}\right) + \left(|m|\frac{\Delta y}{|y|}\right) \dots + \left(|p|\frac{\Delta z}{|z|}\right)}$$

Such formulation was used to compute the uncertainties for the Young's modulus computation based on the known uncertainties of the other physical quantities.